CIRP Annals - Manufacturing Technology 73 (2024) 413–416

Contents lists available at ScienceDirect

CIRP Annals - Manufacturing Technology

journal homepage: https://www.editorialmanager.com/CIRP/default.aspx

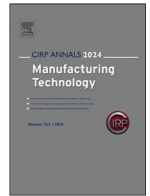

Highly efficient figuring of Si mirrors using an atmosphere plasma jet with concentrated electric field

Hui Deng[a], Bing Wu[a], Junqi Zhang[a], Zhe Zhang[b], Xinquan Zhang (2)[b,*]

[a] *Department of Mechanical and Energy Engineering, Shenzhen Engineering Research Center for Semiconductor-specific Equipment, Southern University of Science and Technology, No. 1088, Xueyuan Road, Shenzhen, Guangdong 518055, China*
[b] *School of Mechanical Engineering, Shanghai Jiao Tong University, Shanghai, 200240, China*

A R T I C L E I N F O

Article history:
Available online 16 May 2024

Keywords:
Plasma
Accuracy
Figuring

Si mirrors with nanometre-level accuracy are required for enhancing X-ray focusing performance but suffer from low manufacturing efficiency. Hereto, a new capacitively coupled plasma jet with a concentrated electric field is developed for highly efficient figuring of Si mirrors. The experimental results show that a high material removal rate, a stable removal function and strong linearity between removal volume and dwell time are realized. The form error of a 100×50 mm^2 Si mirror can be reduced from 110.4 to 7.4 nm RMS within 36.5 min. This work provides a new strategy for the high-efficiency figuring of Si mirrors.

© 2024 CIRP. Published by Elsevier Ltd. All rights are reserved, including those for text and data mining, AI training, and similar technologies.

1. Introduction

Silicon (Si)-based X-ray focusing mirrors are required by synchrotron radiation facilities and free electron laser sources. To improve the focusing performance, the form accuracy of Si mirrors must be improved to the nanometre level [1], and high-accuracy mirrors are generally fabricated by numerically controlled form correction machining [2,3]. At present, elastic emission machining (EEM) and ion beam figuring (IBF) are the most widely used figuring approaches for Si mirrors [4–6]. However, EEMs and IBFs inevitably suffer from low manufacturing efficiency because material removal for EEMs and IBFs is based on atomic-scale shearing and sputtering. Although a peak-to-valley accuracy below 1.0 nm was already achieved by EEM, its material removal rate (MRR) was only approximately 1.4×10^{-14} m^3/h, and it took more than 16 h for a processed area of 25×21 mm^2 [4,5]. Furthermore, a long processing time of 203.45 min was needed for IBF to reduce the root mean square (RMS) accuracy of a Si mirror (150×20 mm^2) from 93.25 to 1.14 nm, as previously reported [6].

Owing to its advantages, such as high efficiency, damage free and low cost, atmospheric pressure reactive plasma has received widespread attention in ultraprecision machining [7]. In the 1990s, plasma chemical vaporization machining (PCVM) was developed using capacitively coupled plasma (CCP), and the MRR was approximately 0.04 mm^3/min for Si [8,9]. Then, reactive atom plasma (RAP) based on inductively coupled plasma (ICP) was proposed for the efficient figuring of fused silica, and a very high MRR of 9 mm^3/min was demonstrated [10]. Additionally, an atmospheric pressure plasma jet (APPJ) system was designed for the damageless machining of Zerodur substrates [11].

The different plasma ignition mechanisms for figuring of Si-based components are summarized in Fig. 1. For ICP, although it is a typical hot plasma with dense radicals enabling the high removal efficiency of RAP [12], its reaction rate is significantly affected by temperature, leading to deteriorating machining stability with time [13]. For CCP in contact mode (CCP-CM), the stage is grounded, and the substrate acts as a dielectric barrier, as shown in Fig. 1(b); thus, only planar substrates can be processed. Moreover, the glow discharge easily converts into unstable arc discharge when CCP-CM is applied to semiconductors such as Si. In contrast, the grounded electrode is independent of the workpiece in CCP with remote mode (CCP-RM), and the plasma jet is sprayed out from the nozzle, as shown in Fig. 1(c) [11,14]. However, the anode will also be etched because it is covered by plasma, which deteriorates the processing stability. Accordingly, it is highly desirable to develop novel atmosphere plasma devices with improved machining efficiency and stability.

In this paper, a new CCP jet with a concentrated electric field (CCP-CEF), as shown in Fig. 1(d), is developed for the figuring of Si mirrors. Powered and ground electrodes are wedge-shaped and installed outside a ceramic tube. The concentrated electric field and erosion-free electrode configuration result in high intensity and high stability of the glow discharge, as summarized in Fig. 1. The electric

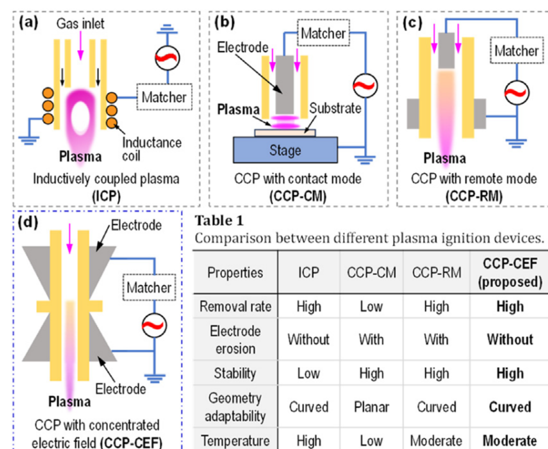

Table 1
Comparison between different plasma ignition devices.

Properties	ICP	CCP-CM	CCP-RM	CCP-CEF (proposed)
Removal rate	High	Low	High	**High**
Electrode erosion	Without	With	With	**Without**
Stability	Low	High	High	**High**
Geometry adaptability	Curved	Planar	Curved	**Curved**
Temperature	High	Low	Moderate	**Moderate**

Fig. 1. Schematics of plasma ignition devices for the figuring process.

* Corresponding author.
E-mail address: zhangxinquan@sjtu.edu.cn (X. Zhang).

https://doi.org/10.1016/j.cirp.2024.04.091
0007-8506/© 2024 CIRP. Published by Elsevier Ltd. All rights are reserved, including those for text and data mining, AI training, and similar technologies.

field and electron density distribution are studied by simulation to understand the plasma ignition process, while the etching behaviours are experimentally evaluated. The figuring performance is further investigated and compared with that of IBFs with the aim of realizing highly efficient and stable figuring for obtaining the nanometre-scale accuracy of Si mirrors.

2. Concept and methodology

Plasma is generated through gas breakdown induced by collisions between accelerated electrons and gas molecules, and gas discharge is likely to occur between the electrodes. Typically, the electric field is concentrated around the edge regions of the electrodes. As shown in Fig. 1(d), a plasma jet could be formed in the customized ceramic tube due to dielectric breakdown of the carrier gas, which is caused by the electric field concentration near the sharp edges of the electrodes. Based on this mechanism, a plasma ignition device composed of CCP-CEF was developed.

A multiphysics simulation was carried out to investigate the distribution of the electric field and electron density for the designed plasma device using COMSOL Multiphysics, as illustrated in Fig. 2(a). Based on a two-dimensional axis-symmetric model, it was found that the wedge-shaped electrode configuration led to an obvious electric field concentration. Electrons were important for the ignition and maintenance of the plasma jet, and they were found to be mainly distributed in the middle area. Fig. 2(b) shows the distribution of the electric field along the centerline of the nozzle. The electric field in the middle area of the two electrodes was much stronger than that in the other areas, which is conducive for plasma generation. Fig. 2(c) shows a photo of the developed CCP-CEF jet device, from which it can be observed that a strong and stable glow discharge was achieved.

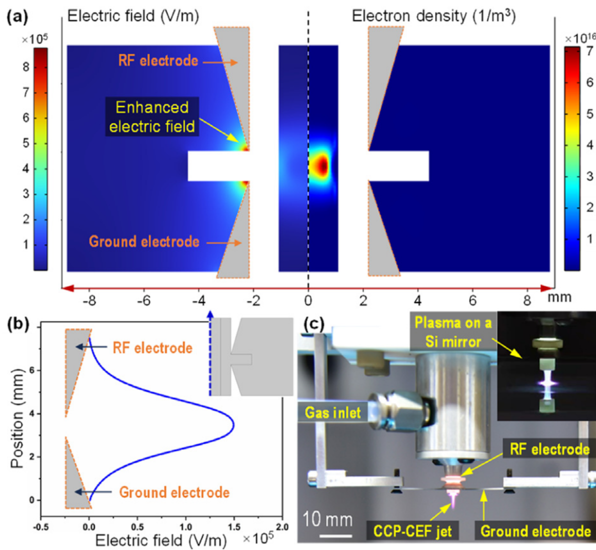

Fig. 2. Multiphysics simulation of the CCP-CEF jet. (a) Distribution of the electric field and electron density. (b) Electric field intensity along the centerline of the nozzle. (c) Photo of the CCP-CEF jet device.

One of the core advantages of CCP-CEF is its high efficiency, which can be revealed through comparison with IBF. As shown in Fig. 3(a) and (b), the MRR of IBF is limited by the ion sputtering yield, while plasma chemical etching can achieve high efficiency by tuning the radical density and temperature. As demonstrated in Fig. 5(c), after static etching for 5 s, a Gaussian-shaped and rotationally symmetrical removal footprint with a full width at half maximum (FWHM) of 3.8 mm was obtained. For comparison, a removal footprint with a similar size (FWHM: 3.6 mm) was obtained by IBF with a 5 mm aperture. The static duration of the IBF was 60 s with a power of 120 W, a working distance of 15 mm, a voltage of 600 V, and an Ar flow rate of 6 sccm. As shown in the cross-section profiles, the depth reached 758.1 nm after CCP-CEF jet etching for 5 s, while it was 66.1 nm after IBF for 60 s. The plasma jet demonstrated a volume removal rate (VRR) of approximately 0.15 mm^3/min, while it was 0.00124 mm^3/min for IBF. Therefore, the VRR of the CCP-CEF jet is more than 100 times larger than that of the IBF with similar FWHMs. Moreover, this value is also much greater than that of CCP-CM and CCP-RM, as previously reported [9,11]. Fig. 3(d) shows the procedure of CCP-CEF jet figuring of an X-ray focusing Si mirror. Similar to other optical figuring techniques, the key process of CCP-CEF jet figuring is the dwell time calculation through the deconvolution algorithm and the numerically controlled plasma machining.

An optical emission spectrometer (*Ocean Optics*, USB2000) was used for the detection of radicals in the CCP-CEF jet. The VRR and form error before and after figuring were measured using a laser interferometer (*Tyggo*, INF150V-LP, reference mirror accuracy: $p\text{-}v<\lambda/20@\lambda=632.8$ nm). For comparison, IBF experiments were conducted using commercial IBF equipment (*ÅFiSy Technology*, IFS1000-600B). The substrate surface temperature in the plasma etching was recorded by an infrared thermal imager (*FLIR*, T660). The process parameters of the CCP-CEF jet are shown in Table 1.

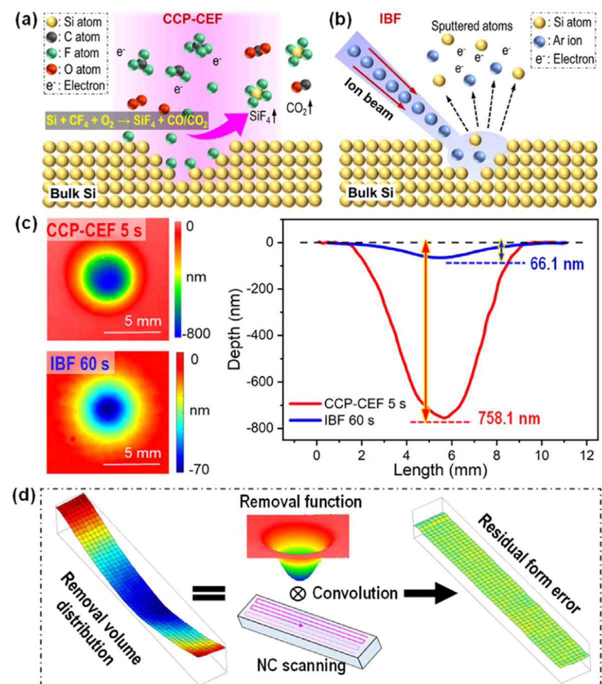

Fig. 3. (a) Schematic of plasma jet etching. (b) Schematic of ion beam sputtering. (c) Removal footprints and cross-sectional profiles of the CCP-CEF jet and IBF. (d) Figuring procedure of a Si mirror by CCP-CEF jet.

Table 1
Experimental parameters of the CCP-CEF jet figuring.

Parameters	Values
Substrate	Si (100): 100×50×10 mm^3, CMP processed
RF frequency	13.56 MHz
RF power	110 W
Flow rates of gas	Carrier gas He: 0.8 slm
	Reactive gas CF_4: 14 sccm/O_2: 4 sccm
Tube diameter	Inner: 2 mm, Outer: 4 mm
Working distance	3 mm

3. Results and discussion

3.1. Diagnostics of the CCP-CEF jet

Optical emission spectrometry (OES) was utilized to evaluate the radical characteristics of the plasma jet. The radical compositions of pure He, He with only CF_4 addition, and He with both O_2 and CF_4 addition were analysed. From the inset optical images of the plasma, strong and uniform glow discharge can be confirmed. Pure He plasma

is mainly composed of peaks corresponding to He and N_2 (from the ambient environment). When CF_4 was added, many peaks originating from the CF_x and C_2 radicals appeared, and the plasma was observed to transform to a greenish colour, where deposition could easily occur. After the addition of oxygen, the intensity of the CF_x and C_2 peaks decreased drastically. Therefore, the addition of oxygen is very useful for promoting the dissociation of CF_x and C_2, and the etching process becomes faster. Fig. 4(b) shows the enlarged spectral range from 620 nm to 760 nm, indicating the presence of a large amount of etchant fluorine radicals.

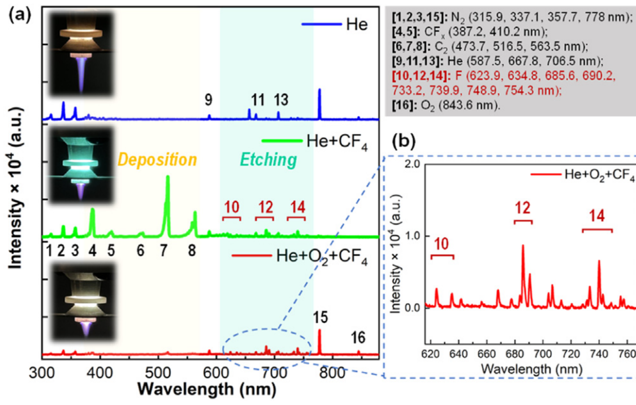

Fig. 4. (a) OES spectra of the plasma with He, He+CF_4 and He+O_2+CF_4 (insets show plasma photos). (b) Enlarged spectra ranging from 620 nm to 760 nm.

3.2. Evaluation of machining characteristics

For optical figuring processes, the removal function stability and the determinacy between dwell time and removal volume strongly affect the figuring accuracy. Fig. 5(a) shows the variation in the CCP-CEF jet removal function. The VRRs of ten independent stationary etching spots with 5 s durations and 5 min intervals were compared to evaluate the stability of the CCP-CEF jet. The removal rate was stable with a variation of ±3.2 %. A similar evaluation was conducted on the IBF process, and the variation in the VRR of the IBF was ±3.0 %. Thus, the developed CCP-CEF jet has comparable removal function stability to that of the commercial IBF. As shown in Fig. 5(b), the correlation between the VRR and plasma dwell time shows a small variation of ±2.6 %, demonstrating the high linearity of the CCP-CEF jet as well as the expected high figuring accuracy of the Si mirrors.

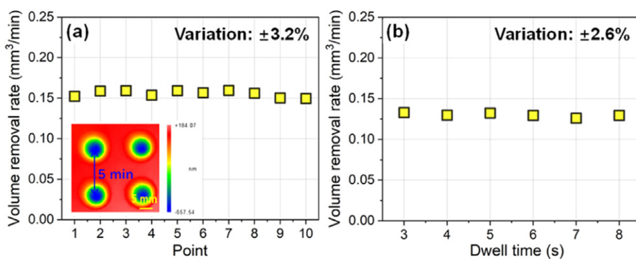

Fig. 5. Experimental stability of the removal function of CCP-CEF. (a) VRRs variation of the stationary spots. (b) VRRs variation with the dwell time.

The correlation between the plasma parameters and the removal rate was investigated to achieve a high figuring efficiency. Fig. 6(a) shows that the VRR gradually increased with increasing CF_4 flow rate. A greater supply of CF_4 will increase the amount of fluorine radicals generated by CF_4 dissociation. As shown in Fig. 6(b), the VRR is sensitive to changes in the O_2 flow rate. The addition of O_2 can effectively promote the production of fluorine radicals and consume carbon-related components such as CF_x, thereby increasing the removal rate. However, an excessive supply of O_2 quenches electrons and radicals, and the VRR decreases [15]. Fig. 6(c) shows the effect of the He flow rate on the VRR. As the carrier gas, excessive He flow rates reduces the effective action time of the fluorine radicals. Fig. 6(d) reveals that RF power is the most efficient parameter for modulating the removal rate. A VRR of 0.19 mm^3/min was obtained when the RF power was 120 W, and the removal rate could be further increased by increasing the RF power. It can be concluded that the CCP-CEF jet developed in this work is a stable and efficient tool for ultraprecision material removal of Si.

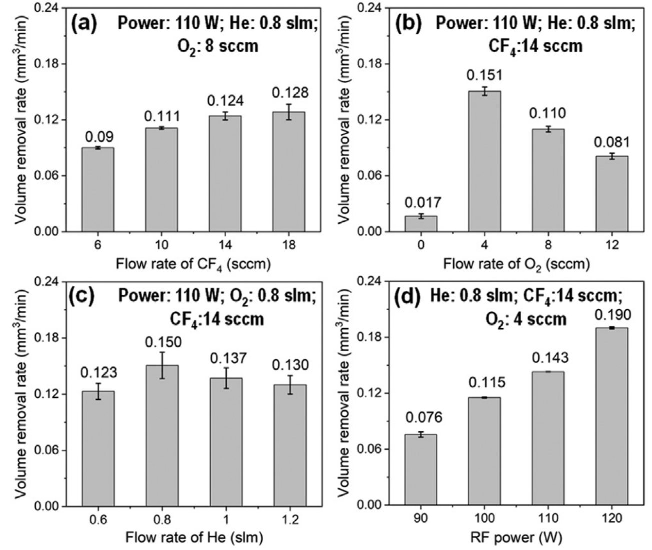

Fig. 6. Parameter optimization of the etching process using the developed CCP-CEF jet. Effect of the CF_4 flow rate (a), O_2 flow rate (b), He flow rate (c), and RF power (d) on the VRR.

3.3. High-efficiency figuring of SI mirrors

In the actual figuring process, the scanning speed changes continuously according to the dwell time. The above VRR was obtained by static etching, which produces a heat accumulation effect. Accordingly, the removal rate should be calibrated through plane-etching calibration, which is similar to the actual figuring process. Theoretically, the calibration results are consistent with the VRR of the actual figuring process at the corresponding speed. The plane-etching area is 65×20 mm^2, and the scanning path is the same as that used in the figuring experiments. The inset in Fig. 7(a) shows the pattern after plane-etching at 300 mm/min. Fig. 7(a) shows the correlation between the VRR and the inverse scanning speed (120–1200 mm/min). The VRR of the plasma jet was constant, with a variation of ±6.4 %, and the average VRR was 0.1 mm^3/min, which is smaller than

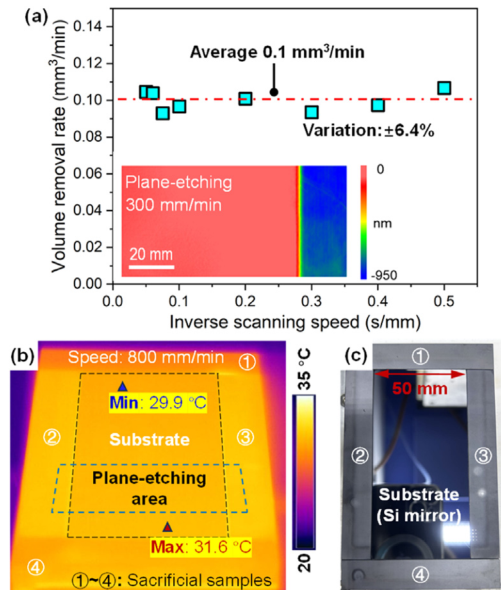

Fig. 7. Calibration of VRR. (a) The VRR versus the inverse scanning speed. (b) Temperature distribution during plane etching. (c) Photo of the Si mirror.

the static VRR. This is because the largest dwell time was 0.5 s/mm, which is much smaller than the 5 s in the static etching experiment.

As illustrated in Fig. 7(b), the constant VRR can be attributed to the insignificant thermal effect during plasma jet scanning of the Si mirror. The thermal conductivity of Si (230 W/mK) is much greater than that of fused silica (1.47 W/mK). Thus, although the thermal effect is severe for plasma figuring of fused silica, the thermal effect during plasma scanning on a Si mirror is negligible. As shown in Fig. 7(c), with the utilization of sacrificial Si substrates, heat rapidly transferred to the whole surface during scanning at 800 mm/min. The minimum and maximum temperatures were 29.9 ℃ and 31.6 ℃, respectively, so the variation was less than 2 ℃ on the whole substrate surface. Therefore, a constant VRR of 0.1 mm^3/min was employed for the calculation of the dwell time in the CCP-CEF jet figuring experiments.

The photo in Fig. 8(a) shows the in-house-developed CCP-CEF jet figuring apparatus. A Si mirror with dimensions of 100×50 mm^2 was fixed on a precision three-axis platform, and the scanning was numerically controlled. A mixture of He with O_2 and CF_4 was supplied through the ceramic tube with the flow rates modulated by mass flow controllers.

The figuring performance of the CCP-CEF jet was verified, and the results are shown in Fig. 8(b) and (c). Fig. 8(b) shows the form error of the Si mirrors before and after plasma figuring. An upright placed laser interferometer was used, and the substrate was fixed on the holder. Three sets of form error data were measured each time, and each set was the average of 10 measurements to reduce interference from vibration and airflow. The RMS value of the form accuracy for the as-received surface is 110.4 nm. After three rounds of figuring via the CCP-CEF jet, the form error was reduced to 7.4 (± 0.072 nm) nm RMS. Fig. 8(c) shows the comparison between the plasma jet figuring and IBF results. A 10 mm aperture with a higher figuring efficiency was used in the IBF experiment. The experimental VRR reached 0.014 mm^3/min at a power of 120 W, a working distance of 20 mm, a voltage of 800 V, and an Ar flow rate of 6 sccm. After 3 rounds of IBF, the RMS was reduced to 3.2 nm, with a processing time of 230.5 min. In comparison, only 36.5 min was needed for the CCP-CEF jet to reach a comparable form accuracy, and this result demonstrated the high efficiency of the developed plasma jet.

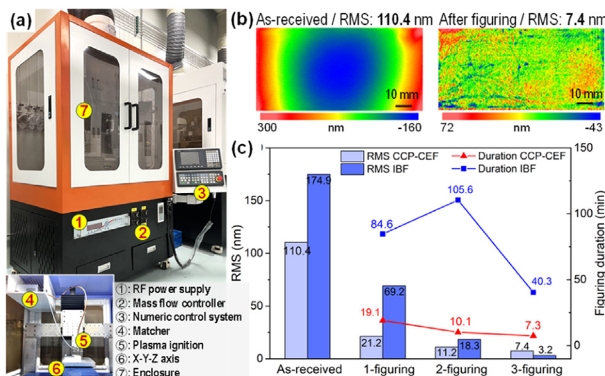

Fig. 8. (a) Photo of the plasma figuring apparatus. (b) Form errors before and after the CCP-CEF jet figuring. (c) RMS evolution and figuring duration of the CCP-CEF jet figuring and IBF.

4. Summary

A capacitively coupled plasma jet with a concentrated electric field was developed and applied for highly efficient figuring of Si mirrors. The localized strong electric field and erosion-free electrode configuration enable the high efficiency and stability of the plasma jet. A removal rate of 0.15 mm^3/min was obtained, which was more than 100 times greater than that of IBFs with similar removal spot sizes. The stability of the removal function (±3.2 %) and the high linearity between the dwell time and removed volume (±2.6 %) were demonstrated. For a 100 × 50 mm^2 Si mirror, the form error rapidly decreased from 110.4 nm to 7.4 nm RMS within 36.5 min, demonstrating the high efficiency of the developed CCP-CEF jet in the manufacturing of large size Si mirrors for X-ray focusing.

Declaration of competing interest

The authors declare that they have no known competing financial interests or personal relationships that could have appeared to influence the work reported in this paper.

CRediT authorship contribution statement

Hui Deng: Conceptualization, Writing – review & editing, Writing – original draft. **Bing Wu:** Data curation, Writing – original draft. **Junqi Zhang:** Methodology, Investigation. **Zhe Zhang:** Methodology, Investigation. **Xinquan Zhang:** Validation, Writing – review & editing.

Acknowledgements

This work received support from the national natural science foundation of China (52035009, 52375437) and the Shenzhen engineering research center for semiconductor-specific equipment.

References

[1] Mimura H, Handa S, Kimura T, Yumoto H, Yamakawa D, Yokoyama H, Matsuyama S, Inagaki K, Yamamura K, Sano Y (2010) Breaking the 10 nm Barrier in Hard-X-Ray Focusing. *Nature Physics* 6(2):122–125.
[2] Beaucamp A, Namba Y (2013) Super-Smooth Finishing of Diamond Turned Hard X-Ray Molding Dies by Combined Fluid Jet and Bonnet Polishing. *CIRP Annals - Manufacturing Technology* 62(1):315–318.
[3] Wang C, Cheung C, Ho L, Liu M, Lee W (2017) A Novel Multi-Jet Polishing Process and Tool for High-Efficiency Polishing. *International Journal of Machine Tools and Manufacture* 115:60–73.
[4] Mimura H, Yumoto H, Matsuyama S, Koyama T, Tono K, Inubushi Y, Togashi T, Sato T, Kim J, Fukui R, Sano Y, Yabashi M, Ohashi H, Ishikawa T, Yamauchi K (2014) Generation of 10^{20}Wcm^{-2} hard X-Ray Laser Pulses with Two-Stage Reflective Focusing System. *Nature Communications* 5(1):3539.
[5] Yumoto H, Koyama T, Suzuki A, Joti Y, Niida Y, Tono K, Bessho Y, Yabashi M, Nishino Y, Ohashi H (2022) High-Fluence and High-Gain Multilayer Focusing Optics to Enhance Spatial Resolution in Femtosecond X-Ray Laser Imaging. *Nature Communications* 13(1):5300.
[6] Wang T, Huang L, Zhu Y, Giorgio S, Boccabella P, Bouet N, Idir M (2023) Ion Beam Figuring System for Synchrotron X-Ray Mirrors Achieving sub-0.2-μrad and sub-0.5-nm Root Mean Square. *Nanomanufacturing and Metrology* 6(1):20.
[7] Deng H, Zhang Y, Liang J, Zhang X (2023) Surface Reconstruction of Sapphire at the Atomic Scale Via Chemical-Physical Tuning of atmospheric Plasma. *CIRP Annals - Manufacturing Technology* 72(1). 489–482.
[8] Mori Y, Yamauchi K, Yamamura K, Sano Y (2000) Development of Plasma Chemical Vaporization Machining. *Review of Scientific Instruments* 71(12):225.
[9] Yamamura K, Shimada S, Mori Y (2008) Damage-free improvement of thickness uniformity of quartz crystal wafer by Plasma Chemical Vaporization Machining. *CIRP Annals - Manufacturing Technology* 57(1):567–570.
[10] Castelli M, Jourdain R, Morantz P, Shore P (2012) Rapid Optical Surface Figuring Using Reactive Atom Plasma. *Precision Engineering* 36(3):467–476.
[11] Yao Y, Wang B, Wang J, Jin H, Zhang Y, Dong S (2010) Chemical Machining of Zerodur Material with atmospheric Pressure Plasma Jet. *CIRP Annals - Manufacturing Technology* 59(1):337–340.
[12] Fang ZD, Zhang Y, Li RL, Liang YN, Deng H (2020) An Efficient Approach for Atomic-Scale Polishing of Single-Crystal Silicon Via Plasma-Based Atom-Selective Etching. *International Journal of Machine Tools and Manufacture* 159:103649.
[13] Jin Y, Su X, Wang B, Li D, Ding F, Qiao Z (2021) The Design and Analysis of a Novel Low Power Atmospheric Plasma Jet Torch for Optical Fabrication. *Journal of Manufacturing Process* 69:422–433.
[14] Li Z, Wang R, Zhang X, Ren M, Zhu L (2023) B-Spline Surface Approximation Method for Achieving Optimum Dwell Time in Deterministic Polishing. *Journal of Materials Processing Technology* 318:118031.
[15] Mogab C, Adams A, Flamm D (1978) Plasma Etching of Si and SiO2-The Effect of Oxygen Additions to CF4 Plasmas. *Journal of Applied Physics* 49(7):3796–3803.